


# Solvable periodic Anderson model with infinite-range Hatsugai-Kohmoto interaction: Ground-states and beyond

Yin Zhong <sup>\*</sup>

*School of Physical Science and Technology & Key Laboratory for Magnetism and  
Magnetic Materials of the MoE, Lanzhou University, Lanzhou 730000, China*

*and Lanzhou Center for Theoretical Physics, Key Laboratory of Theoretical Physics of Gansu Province, Lanzhou 730000, China*



(Received 30 August 2022; revised 29 September 2022; accepted 29 September 2022; published 10 October 2022)

In this paper we introduce a solvable two-orbital (two-band) model with an infinite-range Hatsugai-Kohmoto interaction, which serves as a modified periodic Anderson model. Its solvability results from strict locality in momentum space and is valid for arbitrary lattice geometry and electron filling. A case study of a one-dimensional chain shows that the ground-states have a Luttinger-theorem-violating non-Fermi-liquid-like metallic state, a hybridization-driven insulator, and an interaction-driven featureless Mott insulator. The involved quantum phase transition between metallic and insulating states belongs to the universality of the Lifshitz transition, i.e., a change of topology of the Fermi surface or band structure. Further investigation on a two-dimensional square lattice indicates its similarity with the one-dimensional case, thus the findings in the latter may be generic for all spatial dimensions. We hope the present model or its modification may be useful for understanding novel quantum states in  $f$ -electron compounds, particularly the topological Kondo insulator candidates  $\text{SmB}_6$  and  $\text{YbB}_{12}$ .

DOI: [10.1103/PhysRevB.106.155119](https://doi.org/10.1103/PhysRevB.106.155119)

## I. INTRODUCTION

Recently, solvable quantum many-body systems such as Sachdev-Ye-Kitaev, Kitaev's toric code and honeycomb model have attracted great interest due to emergent novel non-Fermi-liquid and quantum spin liquid states [1–10]. Among them, an infinite-range interaction model without any quenched disorder or local gauge structure called the Hatsugai-Kohmoto (HK) model has been revisited [11–25]. The original HK model provides a strictly exact example for non-Fermi liquid and featureless Mott insulators in any spatial dimension, which is rare in statistical mechanics and condensed-matter physics. The solvability of the HK model results from its locality in momentum space, and one can diagonalize the HK Hamiltonian (only a  $4 \times 4$  matrix) for each momentum. The current studies mainly focus on an interesting extension of the HK model, i.e., the superconducting instability from the intrinsic non-Fermi-liquid state in the HK model [16] (note, however, a study on Kondo impurity in the HK model [20]) and unexpected properties (compared with standard Bardeen-Cooper-Schrieffer (BCS) model [26]) have been discovered, e.g., the emergence of topological  $s$ -wave pairing, two-stage superconductivity, tricritical points, and absence of the Hebel-Slichter peak [18,19,23].

In this paper, we introduce another extension of the HK model, i.e., a two-orbital (two-band) lattice electron system which can be considered as a modified periodic Anderson

model (PAM),

$$\begin{aligned} \hat{H} = & - \sum_{i,j,\sigma} t_{ij}^c \hat{c}_{i\sigma}^\dagger \hat{c}_{j\sigma} - \sum_{i,j,\sigma} t_{ij}^f \hat{f}_{i\sigma}^\dagger \hat{f}_{j\sigma} + E_f \sum_{j\sigma} \hat{f}_{j\sigma}^\dagger \hat{f}_{j\sigma} \\ & + V \sum_{j\sigma} (\hat{c}_{j\sigma}^\dagger \hat{f}_{j\sigma} + \hat{f}_{j\sigma}^\dagger \hat{c}_{j\sigma}) - \mu \sum_{j\sigma} (\hat{c}_{j\sigma}^\dagger \hat{c}_{j\sigma} + \hat{f}_{j\sigma}^\dagger \hat{f}_{j\sigma}) \\ & + \frac{U}{N_s} \sum_{j_1, j_2, j_3, j_4} \delta_{j_1+j_3=j_2+j_4} \hat{f}_{j_1\uparrow}^\dagger \hat{f}_{j_2\uparrow} \hat{f}_{j_3\downarrow}^\dagger \hat{f}_{j_4\downarrow}. \end{aligned} \quad (1)$$

Here,  $\hat{c}_{j\sigma}^\dagger$  is the creation operator of conduction electron ( $c$  electron) while  $\hat{f}_{j\sigma}^\dagger$  denotes an  $f$  electron at site  $j$ .  $t_{ij}^c$  and  $t_{ij}^f$  are hopping integrals between sites  $i, j$  for  $c$  and  $f$  electrons, respectively. Note that  $t_{ij}^f$  is zero in the standard PAM and the  $f$  electron is strictly local in that case, so one may call it a local electron [27].  $E_f$  is the energy level of the  $f$  electron and the hybridization strength between  $c$  and  $f$  electrons is  $V$ . (A spin- and site-dependent  $V$  is also permitted and leads to a nontrivial quantum topological phase such as a topological Kondo insulator [28–32] or a Kondo liquid with a hybridization node [33,34]) Furthermore, the chemical potential  $\mu$  has been added to fix the electron density.  $N_s$  is the number of sites. The last term of  $\hat{H}$  is the less unfamiliar HK interaction [11] (unlike the usual Hubbard interaction  $U \sum_j \hat{f}_{j\uparrow}^\dagger \hat{f}_{j\uparrow} \hat{f}_{j\downarrow}^\dagger \hat{f}_{j\downarrow}$  in standard PAM), which is an infinite-range interaction between four electrons but preserves the center of motion for the  $f$  electron due to the constraint of a  $\delta$  function. This interaction plays a fundamental role in solving this model, as we see later.

Importantly, Eq. (1) is local in momentum space after Fourier transformation, and the resultant Hamiltonian reads

<sup>\*</sup>zhongy@lzu.edu.cn

as  $\hat{H} = \sum_k \hat{H}_k$ , with

$$\begin{aligned} \hat{H}_k = & \sum_{\sigma} (\varepsilon_k^c - \mu) \hat{c}_{k\sigma}^{\dagger} \hat{c}_{k\sigma} + \sum_{\sigma} (\varepsilon_k^f + E_f - \mu) \hat{f}_{k\sigma}^{\dagger} \hat{f}_{k\sigma} \\ & + V \sum_{\sigma} (\hat{c}_{k\sigma}^{\dagger} \hat{f}_{k\sigma} + \hat{f}_{k\sigma}^{\dagger} \hat{c}_{k\sigma}) + U \hat{f}_{k\uparrow}^{\dagger} \hat{f}_{k\uparrow} \hat{f}_{k\downarrow}^{\dagger} \hat{f}_{k\downarrow}, \quad (2) \end{aligned}$$

where  $\varepsilon_k^c$ ,  $\varepsilon_k^f$  are the dispersion of electrons. It is emphasized that the locality of the above Hamiltonian stems from infinite-range HK interaction preserving the center of motion. In contrast, the Hubbard interaction in momentum space is rather nonlocal as  $U \sum_{k,k',q} \hat{f}_{k+q\uparrow}^{\dagger} \hat{f}_{k\uparrow} \hat{f}_{k'-q\downarrow}^{\dagger} \hat{f}_{k'\downarrow}$ , so it cannot lead to the simple formalism in our model.

Now, if we choose the Fock state

$$|n_1, n_2, n_3, n_4\rangle \equiv (\hat{c}_{k\uparrow}^{\dagger})^{n_1} |0\rangle (\hat{c}_{k\downarrow}^{\dagger})^{n_2} |0\rangle (\hat{f}_{k\uparrow}^{\dagger})^{n_3} |0\rangle (\hat{f}_{k\downarrow}^{\dagger})^{n_4} |0\rangle, \quad (3)$$

with  $n_i = 0, 1$  as basis,  $\hat{H}_k$  can be written as a block-diagonal  $16 \times 16$  matrix and a direct numerical diagonalization gives 16 eigenenergies  $E_k(i)$  and eigenstates  $\psi_k(i)$  [ $i = 1, 2, \dots, 16$  and  $|\psi_k(1)\rangle$  is the ground-state for each  $\hat{H}_k$ ]. Details on  $\hat{H}_k$ 's matrix is shown in Appendix A.

Therefore, the many-body ground-state of  $\hat{H}$  is just the direct product state of each  $\hat{H}_k$ 's ground-state, i.e.,  $|\Psi_g\rangle = \prod_k |\psi_k(1)\rangle$  with the corresponding ground-state energy  $E_g = \sum_k E_k(1)$ . Similarly, excited states and their energy are easy to construct, so our model  $\hat{H}$  [Eq. (1)] has been solved since all eigenstates and eigenenergies are found.

Note that the solvability of our model involves only locality in momentum space, therefore Eq. (1) is solvable for an arbitrary lattice geometry, spatial dimension, and electron filling, in contrast with the standard PAM, where a notorious fermion minus-sign problem and the growth of quantum entanglement beyond area law prevent an exact solution or a reliable numerical simulation [35–37]. Furthermore, our solvable model does not rely on disorder average and the large- $N$  limit, which are crucial in the classic Sherrington-Kirkpatrick spin-glass model and the more recent Sachdev-Ye-Kitaev model [1–3,38]. In addition, including pairing terms like  $\hat{c}_{k\uparrow}^{\dagger} \hat{c}_{-k\downarrow}^{\dagger}$ ,  $\hat{f}_{k\uparrow}^{\dagger} \hat{f}_{-k\downarrow}^{\dagger}$ , or  $\hat{c}_{k\uparrow}^{\dagger} \hat{f}_{-k\downarrow}^{\dagger}$  as done in previous studies on the superconductivity of HK [16,18,19] does not change the solvability but only enlarges the dimension of the Hamiltonian in momentum space.

The remaining part of this article is organized as follows: In Sec. II, we study a one-dimensional (1D) chain from our model and establish its ground-state diagram. Several physical quantities like the particle density distribution, density of states, the spectral function, and the Luttinger integral are calculated to characterize possible states. Section III is devoted to discussions, i.e., the case study on a two-dimensional (2D) square lattice and the relation between particle density and metallic states. A brief summary is given in Sec. IV and we also suggest a modification of our model that may be relevant to understand the strong-coupling physics in topological Kondo insulators.

## II. AN EXPLICIT EXAMPLE: THE 1D MODEL

### A. The ground-state

Now, to extract the physics of our model, we focus on its 1D version (extension to other lattices is straightforward), whose Hamiltonian reads as follows:

$$\begin{aligned} \hat{H} &= \sum_k \hat{H}_k, \\ \hat{H}_k &= \sum_{\sigma} (\varepsilon_k - \mu) \hat{c}_{k\sigma}^{\dagger} \hat{c}_{k\sigma} + \sum_{\sigma} (E_f - \mu) \hat{f}_{k\sigma}^{\dagger} \hat{f}_{k\sigma} \\ &+ V \sum_{\sigma} (\hat{c}_{k\sigma}^{\dagger} \hat{f}_{k\sigma} + \hat{f}_{k\sigma}^{\dagger} \hat{c}_{k\sigma}) + U \hat{f}_{k\uparrow}^{\dagger} \hat{f}_{k\uparrow} \hat{f}_{k\downarrow}^{\dagger} \hat{f}_{k\downarrow}, \quad (4) \end{aligned}$$

where  $\varepsilon_k = -2t \cos k$  is the 1D dispersion from nearest-neighbor-hopping  $t$  and the  $f$  electron's dispersion is not included as in standard PAM. To be specific, we set  $t = V = 1$  as the energy unit (a smaller  $V$  is more relevant to experiments in heavy fermion systems but the physics are not changed) and change  $E_f$ ,  $\mu$ ,  $U$  to explore the ground-state phase diagram.

To characterize possible ground-state phases, we calculate some physical observable, e.g., the particle distribution function  $n_k = \langle \hat{n}_k \rangle$  [ $\hat{n}_k = \hat{n}_k^c + \hat{n}_k^f = \sum_{\sigma} (\hat{c}_{k\sigma}^{\dagger} \hat{c}_{k\sigma} + \hat{f}_{k\sigma}^{\dagger} \hat{f}_{k\sigma})$  and  $\langle \dots \rangle$  is chosen as an average over  $|\psi_k(1)\rangle$  if we focus on the ground-state properties], the density of state (DOS) of the  $c$  electron,  $N_c(\omega)$ , the  $f$  electron,  $N_f(\omega)$ , and the total density of states,  $N(\omega)$ , and the spectral function of the  $c$  electron,  $A_c(k, \omega)$ , and of the  $f$  electron,  $A_f(k, \omega)$ .

To calculate the quantities mentioned, we first define the retarded Green's function for the  $c$  electron in the Heisenberg picture as  $G_{\sigma}^c(k, t) = -i\theta(t) \langle [\hat{c}_{k\sigma}(t), \hat{c}_{k\sigma}^{\dagger}]_+ \rangle$ . [ $\theta(x) = 1$  for  $x > 0$  and vanishes if  $x < 0$ ]. Then, its Fourier transformation is denoted  $G_{\sigma}^c(k, \omega)$ , which has the following Lehmann spectral representation [39]:

$$\begin{aligned} G_{\sigma}^c(k, \omega) &= \sum_{j=1}^{16} \frac{|\langle \psi_k(1) | \hat{c}_{k\sigma} | \psi_{k\sigma}(j) \rangle|^2}{\omega + i0^+ + E_k(1) - E_k(j)} \\ &+ \sum_{j=1}^{16} \frac{|\langle \psi_k(1) | \hat{c}_{k\sigma}^{\dagger} | \psi_k(j) \rangle|^2}{\omega + i0^+ + E_k(j) - E_k(1)}. \end{aligned}$$

At the same time, the retarded Green's function for the  $f$  electron has an identical formalism with the simple replacement  $\hat{c}_{k\sigma} \rightarrow \hat{f}_{k\sigma}$ . Therefore,  $A_c(k, \omega) = \sum_{\sigma} A_c^{\sigma}(k, \omega) = \sum_{\sigma} -\frac{1}{\pi} \text{Im} G_{\sigma}^c(k, \omega)$ . As for the DOS, we have the relation  $N(\omega) = N_c(\omega) + N_f(\omega) = \frac{1}{N_s} \sum_k [A_c(k, \omega) + A_f(k, \omega)]$ .

In Fig. 1, we fix  $E_f = -2$  and establish a ground-state phase diagram for different  $\mu$  and  $U$  [another choice of  $E_f$  is explored in Appendix B and no physics is changed].

Here, the particle densities  $n = 0, 4$  ( $n = \frac{1}{N_s} \sum_k n_k$ ) correspond to a trivial band insulator with empty or full occupation for each  $k$  state [the corresponding wave-functions are  $\prod_k |0000\rangle_k$ ,  $\prod_k |1111\rangle_k$  if one utilizes the Fock state (3)].

For  $n = 2$ , we observe an insulator dominated by hybridization strength  $V$  and we call it a hybridization insulator (HI). Physically, the origin of the HI can be understood from the  $U = 0$  limit, and one has the following quasiparticle

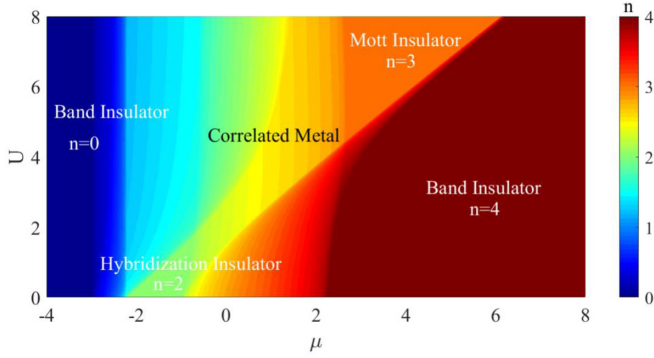


FIG. 1. Ground-state phase diagram of Eq. (4) with fixed  $E_f = -2$ . There exist three kinds of insulating states like band insulator (BI), hybridization insulator (HI), Mott insulator (MI), and one metallic state called correlated metal (CM)

Hamiltonian:

$$\hat{H}_k = \sum_{\sigma} (E_{k+} \hat{\alpha}_{k\sigma}^{\dagger} \hat{\alpha}_{k\sigma} + E_{k-} \hat{\beta}_{k\sigma}^{\dagger} \hat{\beta}_{k\sigma}), \quad (5)$$

with the help of a Bogoliubov transformation  $\hat{\alpha}_{k\sigma} = \mu_k \hat{c}_{k\sigma} + \nu_k \hat{f}_{k\sigma}$  and  $\hat{\beta}_{k\sigma} = -\nu_k \hat{c}_{k\sigma} + \mu_k \hat{f}_{k\sigma}$ . The quasiparticle energy

$$E_{k\pm} = \frac{1}{2} \{ \varepsilon_k + E_f \pm [(\varepsilon_k - E_f)^2 + 4V^2]^{1/2} \} - \mu$$

and

$$\mu_k^2 = \frac{1}{2} \left( 1 + \frac{\varepsilon_k - E_f}{[(\varepsilon_k - E_f)^2 + 4V^2]^{1/2}} \right) = 1 - \nu_k^2.$$

Then, if the lower band  $E_{k-}$  is fully occupied but the upper band  $E_{k+}$  is empty, an insulator (with ground-state wave function  $\prod_{k\sigma} \hat{\beta}_{k\sigma}^{\dagger} |0\rangle$ ) with particle density  $n = 2$  appears, which has an indirect gap  $\approx V$  and a direct gap  $\Delta \equiv \min(E_{k+}) - \max(E_{k-}) \sim V^2/t$ .

Next, let us examine the effect of finite  $U$ . When  $U < \Delta$ , we expect that the gap does not close and the adiabatic principle of Landau applies, thus the system is still in HI but with a renormalized gap and dispersion. Using parameters in our model ( $t = V = 1$ ), we find  $\Delta \approx 1$  and the HI is stable if  $U < \Delta \approx 1$ . This is indeed the case in Fig. 1 and we think the above picture is justified. Furthermore, the ground-state of HI is unique for finite  $U$  and no energy-level crossing appears (see Appendix A for details). In addition, we note that, in the standard PAM, the HI evolves into the antiferromagnetic insulator (on a square lattice) or Kondo insulator when the Hubbard  $U$  increases from  $U = 0$  [35]. Next, we turn to the  $n = 3$  regime, which is clearly driven by the interaction and can be denoted a Mott insulator (MI). From Fig. 2(b), we see that, in a MI, the particle density distribution  $n_k$  is fixed to 3 for each momentum, however, neither  $n_k^c$  nor  $n_k^f$  is fixed to an integer (so this state cannot be an orbital-selective Mott insulator by definition [40]), which should be compared with those in the HI [Fig. 2(a)].

Furthermore, Fig. 3 shows the DOS in the HI [Fig. 3(a)] and MI [Fig. 3(b)]. Although both the MI and HI have a noticeable gap near  $\omega = 0$ , it is clear that a larger gap opens in the MI than in the HI and the former exhibits strong asymmetry for its DOS. Actually, a closer look at the MI's spin-resolved DOS in Figs. 4(a) and 4(b) implies

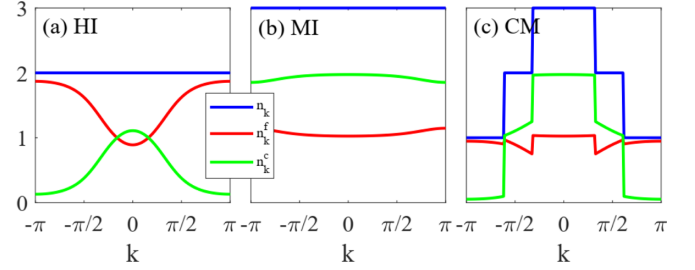


FIG. 2. Particle density distribution  $n_k$ ,  $n_k^f$ , and  $n_k^c$  versus momentum  $k$  with  $E_f = -2$ . (a) HI with  $U = 0.5$ ,  $\mu = -1.3$ . (b) MI with  $U = 6$ ,  $\mu = 3$ . (c) CM with  $U = 6$ ,  $\mu = 0$ .

that the DOS above the Fermi energy ( $\omega = 0$ ) is dominated by spin-down electrons while the  $\omega < 0$  part is contributed to mainly by spin-up electrons. This property seems to be the generic feature for HK-like models. Instead, as can be seen in Figs. 4(c) and 4(d), the spin degrees of freedom are degenerate in HI [see, e.g., the quasiparticle Hamiltonian (5)] and they contribute equally to the DOS ( $N_f^{\uparrow} = N_f^{\downarrow}$ ,  $N_c^{\uparrow} = N_c^{\downarrow}$  in the HI). The spectral function of the  $c$  and  $f$  electrons,  $A_{c/f}(k, \omega) = \sum_{\sigma} A_{c/f}^{\sigma}(k, \omega)$ , is plotted in Figs. 5 and 6. We checked that the spin-resolved spectral function  $A_c^{\sigma}$ ,  $A_f^{\sigma}$  satisfy the sum rule  $\int_{-\infty}^{\infty} d\omega A_{c/f}^{\sigma}(k, \omega) = 1$ . It is observed that, in a MI [Figs. 5(b) and 6(b)] the  $c$  electron has a dispersive band below the Fermi energy ( $\omega = 0$ ) while a rather flat band appears above the Fermi energy for the  $f$  electron. In contrast, two dispersive bands exist near the Fermi energy for both the  $c$  and  $f$  electrons in the HI [Figs. 5(a) and 6(a)], which embody the well-defined quasiparticle band  $E_{k\pm}$ . Finally, the remaining state in the phase diagram is just the metallic state, which is denoted ‘‘correlated metal’’ (CM). The typical particle-density distribution of CM is shown in Fig. 2(c). It is found that, in contrast with Fermi Liquid (FL) or more simply the Fermi gas,  $n_k$  (also for  $n_k^c$ ,  $n_k^f$ ) exhibits two-jump behavior at a certain momentum (one may call it the Fermi point), whose structure is comparable with the non-Fermi-liquid state in the HK model [11]. Therefore, it indicates that a CM should not be a FL but a non-Fermi liquid. The corresponding DOS and the spectral function of CM are investigated in Figs. 3(c), 5(c), and 6(c), and an interesting multiband structure is visible, although we have not found any analytical expression to explain this structure. (According to Appendix A, we have 11

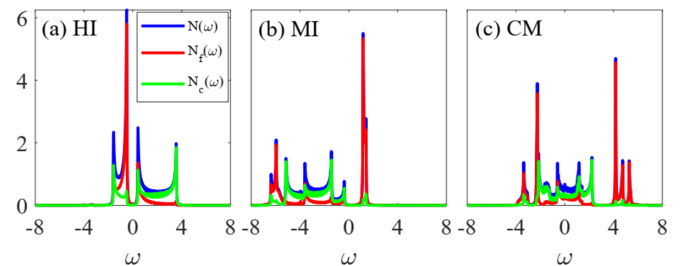


FIG. 3. Density of states  $N(\omega)$ ,  $N_f(\omega)$ , and  $N_c(\omega)$  with  $E_f = -2$ . (a) HI with  $U = 0.5$ ,  $\mu = -1.3$ . (b) MI with  $U = 6$ ,  $\mu = 3$ . (c) CM with  $U = 6$ ,  $\mu = 0$ .

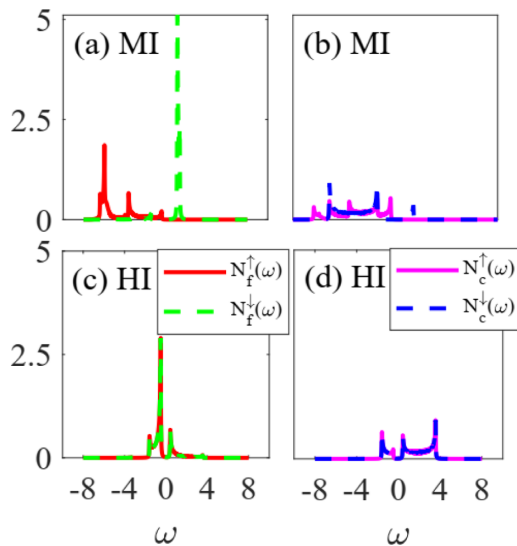


FIG. 4. The spin-resolved density of states for  $f$  and  $c$  electrons,  $N_f^\uparrow(\omega)$ ,  $N_f^\downarrow(\omega)$ ,  $N_c^\uparrow(\omega)$ ,  $N_c^\downarrow(\omega)$  with  $E_f = -2$ . (a), (b) MI with  $U = 6$ ,  $\mu = 3$ . (c), (d) HI with  $U = 0.5$ ,  $\mu = -1.3$ .

different energy level for each  $k$ , thus there exist at most 11 band-like structure in DOS or spectral function.)

To encode the nature of CM, we examine whether CM satisfies the Luttinger theorem [41–44], which has been believed to be defining feature of FL. The Luttinger theorem tells us that, for FL-like states (including a Luttinger liquid in 1D), the following integral, i.e., the Luttinger integral, must be equal to the particle density [45] (here we use its 1D version):

$$I_{LI} = \sum_{\sigma} \int \frac{dk}{2\pi} \theta(\text{Re}G_{\sigma}(k, \omega = 0)). \quad (6)$$

In above formula, the  $\theta$  function counts the positive part of the real part of the retarded Green's function at zero frequency. In our case, we have two Luttinger integrals  $I_{LI}^c$ ,  $I_{LI}^f$  for  $c$  and  $f$  electron. In Fig. 7, we have plotted  $I_{LI}^c$ ,  $I_{LI}^f$  versus particle density ( $n_c$ ,  $n_f$ ) for different chemical potential  $\mu$  with fixed  $E_f = -2$ ,  $U = 6$ . It is obvious that  $I_{LI}^c \neq n_c$  and  $I_{LI}^f \neq n_f$ , thus the CM state ( $-3 < \mu < 4$ ) violates the Luttinger theorem and it is indeed a non-Fermi liquid.

A careful reader may notice that  $I_{LI}^c$ ,  $I_{LI}^f$  are nonmonotonic when  $\mu$  changes. A straightforward explanation seems to be that such behavior results from the change of topology of Fermi surface or band structure, i.e., the famous Lifshitz

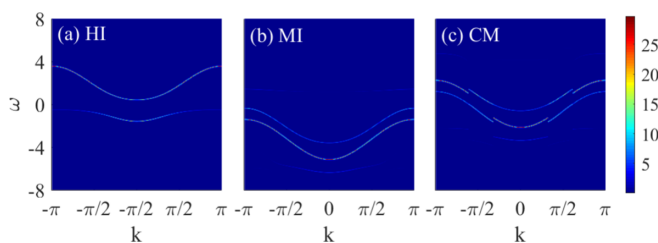


FIG. 5. Spectral function of  $c$  electron,  $A_c(k, \omega)$ , with  $E_f = -2$ . (a) HI with  $U = 0.5$ ,  $\mu = -1.3$ . (b) MI with  $U = 6$ ,  $\mu = 3$ . (c) CM with  $U = 6$ ,  $\mu = 0$ .

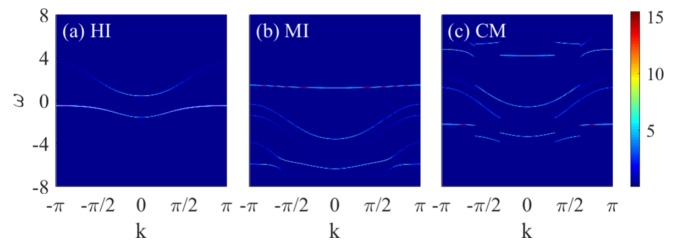


FIG. 6. Spectral function of  $f$  electron  $A_f(k, \omega)$  with  $E_f = -2$ . (a) HI with  $U = 0.5$ ,  $\mu = -1.3$ . (b) MI with  $U = 6$ ,  $\mu = 3$ . (c) CM with  $U = 6$ ,  $\mu = 0$ .

transition. When the Lifshitz transition appears with tuning  $\mu$ , the particle density will show a kink-like structure. In Fig. 7, one see that, when kinks emerge in  $n_c$ ,  $n_f$ , the Luttinger integral  $I_{LI}^c$ ,  $I_{LI}^f$  exhibit strong deviation from Luttinger theorem. Therefore, CM is not a single phase but includes many Lifshitz transitions.

## B. How about the phase transition?

We have explored the ground-state phase diagram and there exist four states, namely, BI, HI, MI, and CM. Except for the trivial BI, we expect quantum transitions between metallic and insulating states (CM-MI and CM-HI). Since there is no explicit candidate, Landau's order parameter with noticeable symmetry breaking, a natural guess, suggests these transitions are of the nature of the Lifshitz transition. One may argue that an alternative explanation can be certain topological order [46–48], but such a possibility in 1D is not plausible since prototypical  $Z_2$  topological order is not stable in 1D unless one ignores the effect of effective electric field in  $Z_2$  lattice gauge field theory [7,49]. The possibility of topological order in the 2D version of our model or other HK-like models has not been explored and we suspect that it will not relate to the models mentioned. After all, in this work, we only examine the Lifshitz transition.

To locate and characterize such a putative transition, we inspect the behavior of the charge susceptibility  $\chi_c = \partial n / \partial \mu$ , which diverges at the critical point driven by charge fluctuation like the Lifshitz transition.

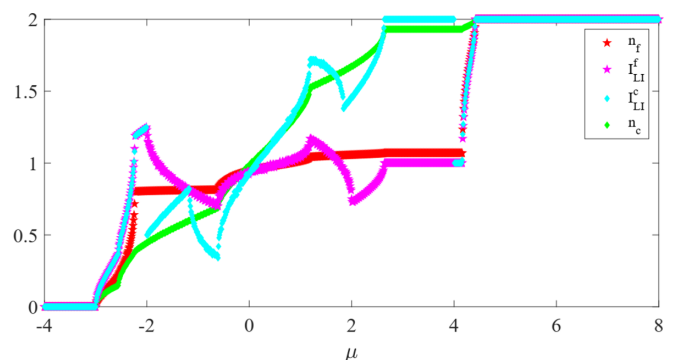


FIG. 7. Luttinger integral ( $I_{LI}^c$ ,  $I_{LI}^f$ ) versus particle density ( $n_c$ ,  $n_f$ ) for different chemical potential  $\mu$  with  $E_f = -2$ ,  $U = 6$ .

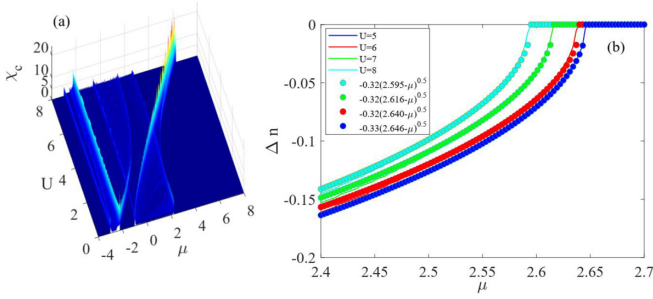


FIG. 8. (a) The charge susceptibility  $\chi_c$  with  $E_f = -2$ . (b) Particle density difference  $\Delta n$  near critical point versus fitted scaling formula Eq. (7) with  $E_f = -2$ .

As can be seen in Fig. 8(a), the divergent  $\chi_c$  is able to locate the phase boundary, which agrees perfectly with our previous phase diagram (Fig. 1).

Now, let us focus on the phase transition between the CM and MI. To be specific, consider  $U = 5, 6, 7, 8$  while tuning  $\mu$  with fixed  $E_f = -2$ . These are the chemical-potential-driven transitions and their critical points are located in  $\mu = \mu_c = 2.595, 2.616, 2.640, 2.646$ . According to general ideas of quantum phase transition, we expect the particle density near the critical point to have the following scaling form [50]:

$$\Delta n = n - n_0 \sim (\mu - \mu_c)^\beta, \quad (7)$$

where  $n_0$  denotes certain background which should be subtracted,  $\mu_c$  is the location of the critical point, and  $\beta$  is the critical exponent. The above scaling formula works well near critical points, as shown in Fig. 8(b), and one finds that  $\beta \simeq 0.5$ , which is the critical exponent for expected Lifshitz transition. ( $\beta = d/2$  for the free fermion Lifshitz transition universality with the dimension of space  $d$  and the dynamic critical exponent  $z = 2$ .) Furthermore, the ground-state energy and charge susceptibility also have the scaling form  $E_g - E_g^0 \sim (\mu - \mu_c)^{(d+2)/2}$ ,  $\chi_c \sim (\mu - \mu_c)^{(d-2)/2}$  [50,51], which are consistent with our calculation if choosing spatial dimension  $d = 1$ . Therefore, we conclude that the chemical potential-driven CM-MI transition is in fact the Lifshitz transition.

One may note that there also exists interaction-driven CM-MI transition. Although we have not explored its properties in detail, based on our knowledge on HK-like models, this transition should belong to the universality of Lifshitz transition as well [50,51]. In addition, it is not surprising to find that the CM-HI transition is of the nature of the Lifshitz transition and we will not investigate it further.

### C. Is there any effective field theory description for a CM, MI, or HI?

In the study of correlated electron systems, the effective (field) theory description is very useful since it can give us the low-energy theory, which is truly responsible for understanding low-temperature or low-frequency thermodynamics and transport [52,53]. Frankly speaking, we have no idea how to construct a suitable effective theory for CM and MI. At this point, one may ask why the state-of-the-art 1D bosonization is not able to attack our model. The reason is that the

Luttinger theorem, which fixes the Fermi point (Fermi surface in 1D) for a given particle density [54], is violated in our model, thus the starting the point of bosonization, i.e., the low-energy expansion around the Fermi point, is meaningless. Consequently, we do not expect the bosonization technique to be useful to our model. [We have also tried to relate a metallic CM to conformal-field-theory (CFT) but have failed since the finite-size scaling of CM in our model is not consistent with well-known CFT models, like minimal models [55]. Alternatively, one may see the interaction in Eq. (4) as a Hubbard interaction in momentum space, thus slave-particle theory like slave-rotor or slave-spin could be used if  $U$  is large [56,57]. However, those slave-particle-mean-field theories give rise to solutions with spin degeneracy in paramagnetic states, which contrasts with the exact result such as the spin-resolved spectral function (Fig. 4), where spin-degeneracy is lost in the CM or MI. Consequently, slave-particle techniques may not be helpful to provide an effective theory for understanding the CM and MI.

Next, one may note that our model is similar to the original HK model, and the latter one has many simple and beautiful analytic results. Thus, if we can project our model into the HK model, life will be easy. Let us try this idea in terms of the path-integral formalism. The imaginary-time action of our model is just like

$$S = \sum_k \int d\tau \sum_\sigma \bar{c}_{k\sigma} (\partial_\tau + \varepsilon_k - \mu) c_{k\sigma} + \sum_\sigma \bar{f}_{k\sigma} (\partial_\tau + E_f - \mu) f_{k\sigma} + V \sum_\sigma (\bar{c}_{k\sigma} f_{k\sigma} + \bar{f}_{k\sigma} c_{k\sigma}) + U \bar{f}_{k\uparrow} f_{k\uparrow} \bar{f}_{k\downarrow} f_{k\downarrow}, \quad (8)$$

where  $\bar{c}_{k\sigma}$ ,  $c_{k\sigma}$ ,  $\bar{f}_{k\sigma}$ ,  $f_{k\sigma}$  are the anticommutative Grassman field. Note that the HK interaction is active for the  $f$  electron, we may integrate the  $c$  electron out to get an  $f$ -electron-only theory. After integrating out the  $c$  electron's degree of freedom, we find the following action for the  $f$  electron:

$$S_f = \sum_k \int d\tau \sum_\sigma \bar{f}_{k\sigma} (\partial_\tau + E_f - \mu) f_{k\sigma} + U \int d\tau \bar{f}_{k\uparrow} f_{k\uparrow} \bar{f}_{k\downarrow} f_{k\downarrow} + \int d\tau \int d\tau' \sum_\sigma \bar{f}_{k\sigma}(\tau) V^2 G_k^0(\tau - \tau') f_{k\sigma}(\tau'). \quad (9)$$

Here,  $G_k^0(\tau)$  is the Fourier transformation of a free  $c$  electron Green's function  $G^0(k, \omega_n) = (i\omega_n - \varepsilon_k + \mu)^{-1}$ . We see that the above action is nonlocal in imaginary time and thus cannot be written as the HK model.

As for HI, in the previous section, we have analyzed its  $U = 0$  limit and argued that it is stable if the gap still opens. Here, motivated by Eq. (8), we treat the HK interaction as a perturbation and the induced correction at first order gives rise to the Hartree self-energy  $\Sigma_\sigma(k, \omega) = U n_{k\bar{\sigma}}^f (n_{k\bar{\sigma}}^f = \langle \bar{f}_{k\bar{\sigma}}^\dagger \hat{f}_{k\bar{\sigma}} \rangle)$  with  $\bar{\sigma} \equiv -\sigma$ . Therefore, we have an  $f$ -electron Green's

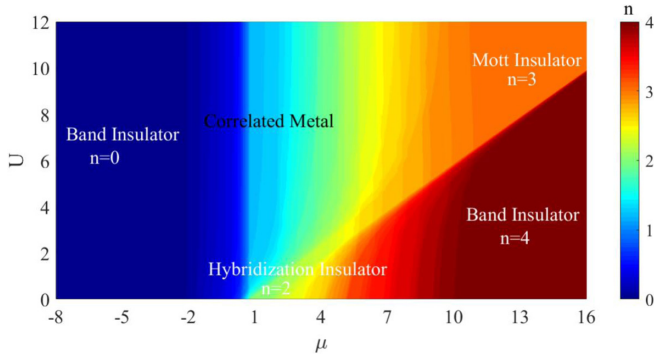


FIG. 9. Ground-state phase diagram of 2D square lattice with fixed  $E_f = -2$ . Note that it is similar to the 1D case of Fig. 1.

function

$$G_\sigma^f(k, \omega) = \frac{1}{(G_0^f(k, \omega))^{-1} - U n_{k\bar{\sigma}}^f}, \quad (10)$$

with  $G_0^f(k, \omega) = [\omega - E_f + \mu - V^2(\omega - \varepsilon_k + \mu)^{-1}]^{-1}$  being the  $f$ -electron Green's function in the  $U = 0$  limit. Now, the pole of  $G_\sigma^f(k, \omega)$  determines the renormalized quasiparticle dispersion, whose form is

$$\tilde{E}_{k\sigma\pm} = \frac{1}{2}[\varepsilon_k + E_f + U n_{k\bar{\sigma}}^f \pm A_{k\sigma}] - \mu, \\ A_{k\sigma} = \sqrt{(\varepsilon_k - E_f)^2 + (U n_{k\bar{\sigma}}^f)^2 + 2U n_{k\bar{\sigma}}^f(3\varepsilon_k + E_f - 4\mu)}.$$

### III. DISCUSSION

#### A. Example on 2D square lattice

In the previous section, we investigated a 1D model and established its phase diagram. In this section, we briefly discuss the properties on a 2D square lattice. For this lattice, the only difference from the 1D model is that the nearest-neighbor hopping for the  $c$  electron generates  $\varepsilon_k = -2t(\cos k_x + \cos k_y)$  instead of  $-2t \cos k$ . Others are the same as our previous discussion.

To get a rough intuition for this 2D problem, we plot its ground-state phase diagram in Fig. 9 with  $t = V = 1$ ,  $E_f = -2$ . The structure of this phase diagram is quite similar to the 1D version of Fig. 1 (including the insulating BI, HI, MI, and metallic CM as in 1D), therefore we expect that the findings in the previous 1D model may be generic for all spatial dimensions.

In addition, we have shown the  $f$  electron's zero-frequency spectral function  $A_f(k_x, k_y, \omega = 0)$  on the 2D square lattice in Fig. 10, which is able to encode the structure of Fermi surface. Obviously, one observes that tuning the chemical potential  $\mu$  drives the transition of the Fermi surface, which is the counterpart of the Lifshitz transition in 2D. The corresponding real part of the  $f$  electron's Green's function at  $\omega = 0$  is shown in Fig. 11, where clear jump from  $-\infty$  to  $\infty$  appears indicates the existence of the Fermi surface. However, we have checked that the Luttinger theorem does not hold in the correlated metal, so the metallic regime is still a non-Fermi liquid although it has the Fermi-surface structure.

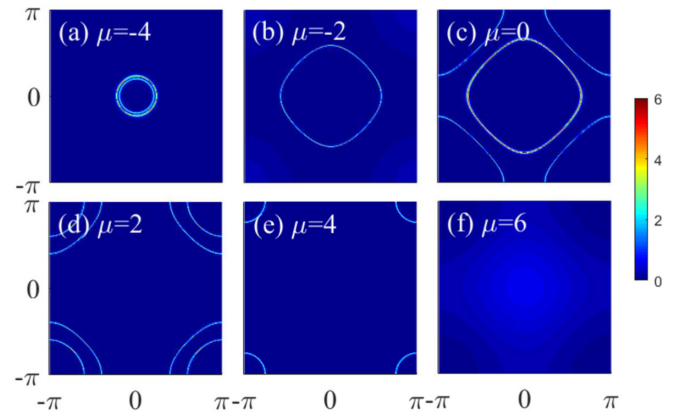


FIG. 10. The  $f$  electron's zero-frequency spectral function  $A_f(k_x, k_y, \omega = 0)$  on a 2D square lattice with  $E_f = -2$ ,  $U = 8$ : (a)  $\mu = -4$ , (b)  $\mu = -2$ , (c)  $\mu = 0$ , (d)  $\mu = 2$ , (e)  $\mu = 4$ , (f)  $\mu = 6$ .

#### B. Relation between particle density and metallic state

We have seen that, in the ground-state of Eq. (4), the particle density of insulating states is an integer ( $n = 0, 2, 3, 4$ ) while the metallic CM is generally not an integer. Here, following the treatment in Ref. [58], which utilizes the classic proof of the Lieb-Schultz-Mattis (LSM) theorem, we provide an intuitive argument on this point.

At first, we rewrite Eq. (4) into its real-space version, whose Hamiltonian reads

$$\hat{H} = -t \sum_{j\sigma} (\hat{c}_{j\sigma}^\dagger \hat{c}_{j+1\sigma} + \hat{c}_{j+1\sigma}^\dagger \hat{c}_{j\sigma}) - \mu \sum_{j\sigma} \hat{c}_{j\sigma}^\dagger \hat{c}_{j\sigma} \\ + \sum_{j\sigma} (E_f - \mu) \hat{f}_{j\sigma}^\dagger \hat{f}_{j\sigma} + V \sum_{j\sigma} (\hat{c}_{j\sigma}^\dagger \hat{f}_{j\sigma} + \hat{f}_{j\sigma}^\dagger \hat{c}_{j\sigma}) \\ + \frac{U}{N_s} \sum_{j_1 j_2 j_3 j_4} \delta_{j_1 + j_3 = j_2 + j_4} \hat{f}_{j_1 \uparrow}^\dagger \hat{f}_{j_2 \uparrow} \hat{f}_{j_3 \downarrow}^\dagger \hat{f}_{j_4 \downarrow}. \quad (11)$$

Then, consider the periodic boundary condition and define the twist operator

$$\hat{U} = e^{i \sum_{j=1}^{N_s} \frac{2\pi j}{N_s} \sum_{\sigma} (\hat{c}_{j\sigma}^\dagger \hat{c}_{j\sigma} + \hat{f}_{j\sigma}^\dagger \hat{f}_{j\sigma})}. \quad (12)$$

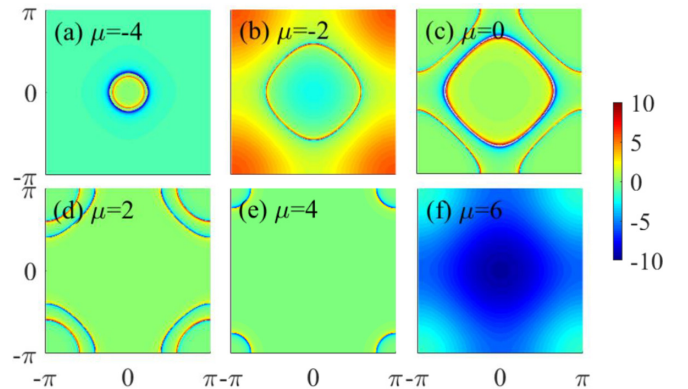


FIG. 11. The real part the  $f$  electron's zero-frequency Green's function  $\text{Re}G_f(k_x, k_y, \omega = 0)$  on a 2D square lattice with  $E_f = -2$ ,  $U = 8$ . (a)  $\mu = -4$ . (b)  $\mu = -2$ . (c)  $\mu = 0$ . (d)  $\mu = 2$ . (e)  $\mu = 4$ . (f)  $\mu = 6$ .

If we denote the ground-state  $|\Psi_0\rangle$ , then a new state is constructed by applying  $\hat{U}$ , i.e., the twisted state  $\hat{U}|\Psi_0\rangle$ . So, one can calculate the energy difference

$$\begin{aligned}\Delta E &= \langle \Psi_0 | \hat{U}^{-1} \hat{H} \hat{U} | \Psi_0 \rangle - \langle \Psi_0 | \hat{H} | \Psi_0 \rangle \\ &= \sum_{\sigma} \sum_{j=1}^{N_s} (2 - e^{-i2\pi/N_s} - e^{i2\pi/N_s}) t (\hat{c}_{j\sigma}^{\dagger} \hat{c}_{j+1\sigma}).\end{aligned}$$

When  $N_s \gg 1$ ,  $\Delta E \approx O(1/N_s)$ , thus there exists at least one low-energy state near the ground-state. Furthermore, for the translation operator  $\hat{T}$ , we have  $\hat{T} \hat{U} \hat{T}^{-1} = \hat{U} e^{-i2\pi \hat{n}}$  [ $\hat{n} = \frac{1}{N_s} \sum_{j\sigma} (\hat{c}_{j\sigma}^{\dagger} \hat{c}_{j\sigma} + \hat{f}_{j\sigma}^{\dagger} \hat{f}_{j\sigma})$ ]. Assume the ground-state  $|\Psi_0\rangle$  has particle density  $n$  and momentum  $P_0$ , then

$$\hat{T} \hat{U} |\Psi_0\rangle = \hat{U} \hat{T} e^{-i2\pi \hat{n}} |\Psi_0\rangle = e^{-i2\pi n} e^{-iP_0} \hat{U} |\Psi_0\rangle, \quad (13)$$

which means that the twisted state is the eigenstate of momentum  $2\pi n + P_0$ . If  $n$  is not an integer,  $\hat{U}|\Psi_0\rangle$  and  $|\Psi_0\rangle$  must be orthogonal, thus the system is gapless in this situation and it corresponds to a metallic state. In contrast, when  $n$  is an integer, we expect that  $\hat{U}|\Psi_0\rangle$  and  $|\Psi_0\rangle$  are the same state, which suggests that there exists no low-energy state and the system should be an insulator. Therefore, we now understand why  $n = 0, 2, 3, 4$  in our model correspond to insulating states and generic electron's density implies metallic state.

#### IV. CONCLUSION AND FUTURE DIRECTIONS

In conclusion, we have provided a solvable quantum many-body model whose solvability is due to locality in momentum space, and we analyzed the ground-state properties in its 1D version. Importantly, we find a non-Fermi-liquid-like metallic state violating the Luttinger theorem and an interaction-driven Mott insulator in the ground-state. The involved quantum phase transition between these two states belongs to the universality of the Lifshitz transition. The phase diagram of the 2D version of our model is similar to 1D and it is expected that the findings in the latter may be generic for all spatial dimensions.

In light of recent theoretical and experimental works on topological Kondo insulators, particularly the unusual quantum oscillation found in  $\text{SmB}_6$  and  $\text{YbB}_{12}$  [59–69], our solvable model can be modified (with momentum- and spin-dependent hybridization strength) to attack topological phases relevant to these interesting  $f$ -electron compounds, for example, a solvable model to give insight into 1D topological Kondo insulators is [70–72]

$$\begin{aligned}\hat{H} &= -t \sum_{j\sigma} (\hat{c}_{j\sigma}^{\dagger} \hat{c}_{j+1\sigma} + \hat{c}_{j+1\sigma}^{\dagger} \hat{c}_{j\sigma}) - \mu \sum_{j\sigma} \hat{c}_{j\sigma}^{\dagger} \hat{c}_{j\sigma} \\ &+ \frac{1}{2} \sum_{j\sigma, \delta=\pm 1} V_{j, j+\delta} (\hat{c}_{j+\delta\sigma}^{\dagger} \hat{f}_{j\sigma} + \hat{f}_{j\sigma}^{\dagger} \hat{c}_{j+\delta\sigma}) \\ &+ E_f \sum_{j\sigma} \hat{f}_{j\sigma}^{\dagger} \hat{f}_{j\sigma} + \frac{U}{N_s} \sum_{j_1 j_2 j_3 j_4} \delta_{j_1+j_3=j_2+j_4} \hat{f}_{j_1\uparrow}^{\dagger} \hat{f}_{j_2\uparrow} \hat{f}_{j_3\downarrow}^{\dagger} \hat{f}_{j_4\downarrow},\end{aligned}$$

with  $V_{j, j+1} = V$ ,  $V_{j, j-1} = -V$ . Such exciting possibilities will be explored in future work and we hope our model will be a good starting point to explore unexpected physics in correlated electron systems.

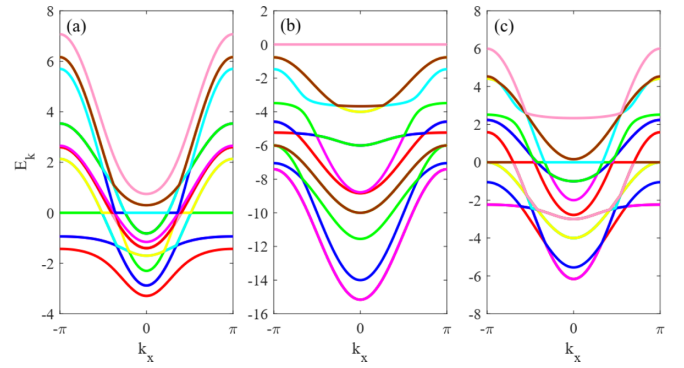


FIG. 12. Eigenenergy  $E_k$  with fixed  $E_f = -2$  for (a) hybridization insulator ( $U = 0.5$ ,  $\mu = -1.3$ ), (b) Mott insulator ( $U = 6$ ,  $\mu = 3$ ), (c) correlated metal ( $U = 6$ ,  $\mu = 0$ ).

#### APPENDIX A: DIAGONALIZATION OF $\hat{H}_k$

Before diagonalizing  $\hat{H}_k$ , we observe that particle number  $\hat{n}_k = \sum_{\sigma} (\hat{c}_{k\sigma}^{\dagger} \hat{c}_{k\sigma} + \hat{f}_{k\sigma}^{\dagger} \hat{f}_{k\sigma})$  and spin  $\hat{S}_k^z = \frac{1}{2} (\hat{c}_{k\uparrow}^{\dagger} \hat{c}_{k\uparrow} - \hat{c}_{k\downarrow}^{\dagger} \hat{c}_{k\downarrow} + \hat{f}_{k\uparrow}^{\dagger} \hat{f}_{k\uparrow} - \hat{f}_{k\downarrow}^{\dagger} \hat{f}_{k\downarrow})$  are both conserved in  $\hat{H}_k$ . Therefore, the  $16 \times 16$  matrix of  $\hat{H}_k$  has the block-diagonal form as  $H_k = 1 \oplus 2 \oplus 2 \oplus 1 \oplus 1 \oplus 4 \oplus 2 \oplus 2 \oplus 1$ . The first 1 means  $|0000\rangle$  with  $n_k = 0$ ,  $S_k^z = 0$  is the eigenstate with eigenenergy 0. The second 2 encodes that

$$H_k = \begin{pmatrix} \xi_k^c & V \\ V & \xi_k^f \end{pmatrix}$$

in the subspace formed by  $|1000\rangle$  and  $|0010\rangle$  with  $n_k = 1$ ,  $S_k^z = 1/2$ . Here, we have introduced  $\xi_k^c = \varepsilon_k^c - \mu$ ,  $\xi_k^f = \varepsilon_k^f + E_f - \mu$  to simplify the expression. The third 3 gives the same  $2 \times 2$  matrix, which is formed by  $|0100\rangle$  and  $|0001\rangle$  with  $n_k = 1$ ,  $S_k^z = -1/2$ . The fourth and fifth 1 produce identical energy  $\xi_k^c + \xi_k^f$  for the  $|1010\rangle$  state with  $n_k = 2$ ,  $S_k^z = 1$  and  $|0, 1, 0, 1\rangle$  state with  $n_k = 2$ ,  $S_k^z = -1$ . Now, we come with the sixth 4, whose subspace is formed by  $|1100\rangle$ ,  $|1001\rangle$ ,  $|0110\rangle$ , and  $|0011\rangle$  with  $n_k = 2$ ,  $S_k^z = 0$ . Therefore,  $\hat{H}_k$  has the following  $4 \times 4$  matrix representation:

$$H_k = \begin{pmatrix} 2\xi_k^c & V & -V & 0 \\ V & \xi_k^c + \xi_k^f & 0 & V \\ -V & 0 & \xi_k^c + \xi_k^f & -V \\ 0 & V & -V & 2\xi_k^f + U \end{pmatrix}. \quad (A1)$$

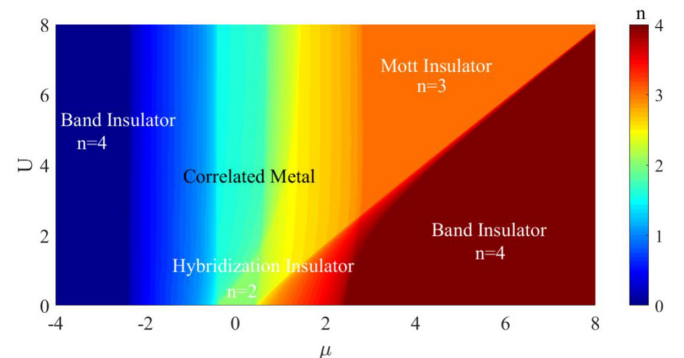
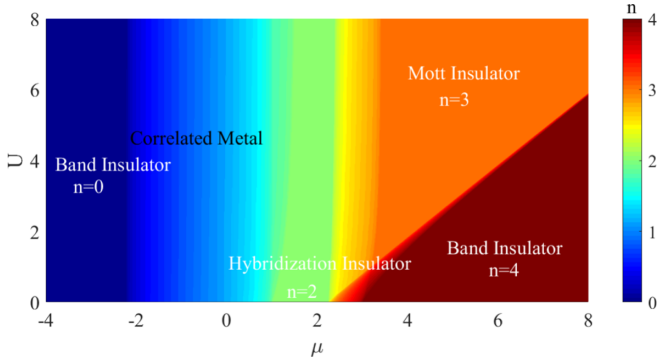


FIG. 13. Ground-state phase diagram of Eq. (3) with fixed  $E_f = 2$ .

FIG. 14. Ground-state phase diagram of Eq. (3) with fixed  $E_f = 0$ .

Although an analytic expression of the eigenenergy and eigenstate is available, it is too complicated to use, so we diagonalize the above matrix numerically.

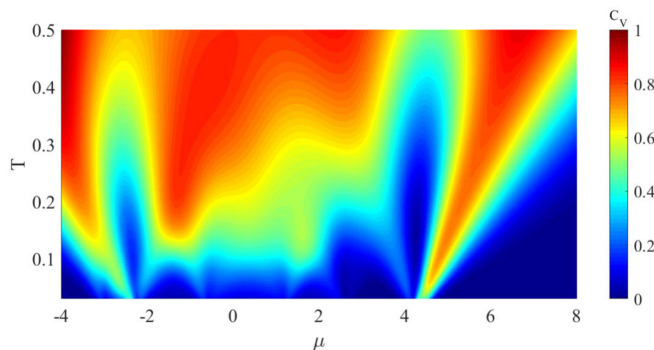
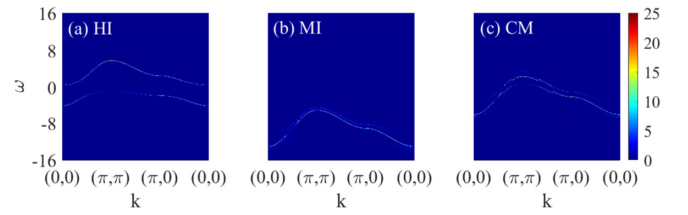
Then, the seventh and eighth 2 give the same

$$H_k = \begin{pmatrix} 2\xi_k^c + \xi_k^f & -V \\ -V & \xi_k^c + 2\xi_k^f + U \end{pmatrix},$$

which is formed by  $|1110\rangle, |1011\rangle$  with  $n_k = 3, S_k^z = 1/2$  and  $|1101\rangle, |0111\rangle$  with  $n_k = 3, S_k^z = -1/2$ , respectively. The last 1 means that the  $|1111\rangle$  state has eigenenergy  $2\xi_k^c + 2\xi_k^f + U$ .

Based on the above results, we conclude that, in terms of Fock states  $|n_1, n_2, n_3, n_4\rangle$  ( $n_i = 0, 1$ ) the Hamiltonian  $\hat{H}_k$  has been diagonalized and we obtain 16 eigenenergies  $E_k(i)$  and eigenstates  $\psi_k(i)$  ( $i = 1, 2, \dots, 16$ ) With the same spirit, one can construct the matrix expression like the fermionic operators  $\hat{c}_{k\sigma}, \hat{f}_{k\sigma}$ , which are useful to calculate the Green's function and spectral function.

In Fig. 12, we have given samples of eigenenergy  $E_k$  for the 1D model in the main text, which is related to the hybridization insulator, Mott insulator, and correlated metal in the main text ( $t = V = 1, E_f = -2$ ). We find that the ground-state of hybridization insulator (HI) is unique and is formed by a mixture of four basis states in the  $n_k = 2, S_k^z = 0$  subspace. If we treat the eigenenergy  $E_k$  as an imaginary band, Fig. 12 can be seen as the evolution of  $E_k$  versus  $k_x$ . Since no energy-level crossing appears, all eigenstates in HI are adiabatically connected. In contrast, the ground-state of the Mott insulator (MI) has a large degeneracy since one can

FIG. 15. The heat capacity  $C_V$  versus  $\mu$  and  $T$  with fixed  $E_f = -2, U = 6$ .FIG. 16. Spectral function of  $c$  electron  $A_c(k, \omega)$  with  $E_f = -2$  on a square lattice. (a) HI with  $U = 0.5, \mu = -1$  (we choose  $V = 2$  to enhance the visibility of HI). (b) MI with  $U = 12, \mu = 10$ . (c) CM with  $U = 6, \mu = 2$ .

use two degenerate  $\psi_k(1), \psi_k(2)$  for each  $k$  to construct a desirable ground-state, which is a general feature of a MI in HK-like models. As for the correlated metal, one observes the appearance of energy level crossing (such crossings can also be checked in terms of fidelity, the overlap of nearby wave-function  $F_{ij}(k, \delta k) = \langle \psi_{k+\delta k}(i) | \psi_k(j) \rangle$  [73,74]) and it explains the two-jump structure in the particle density distribution of Fig. 2(c).

#### APPENDIX B: PHASE DIAGRAM FOR $E_f = 0$ AND $E_f = 2$

Here, we plot the ground-state phase diagram for 1D models with  $E_f = 0$  and  $E_f = 2$  in Figs. 13 and 14. Other parameters are chosen as the  $E_f = -2$  case. We see that the structure of all phase diagrams for  $E_f = -2, 0, 2$  is similar and the generic physics does not change. Additionally, we observe that increasing  $E_f$  has the effect to enlarge the  $n = 2$  HI and  $n = 3$  MI regime.

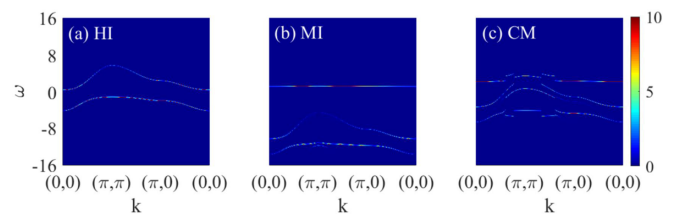
#### APPENDIX C: FINITE TEMPERATURE

After presenting results on the ground-state in the main text, we now study the finite-temperature case. At finite  $T$ , the thermodynamics of our model is determined by its free-energy density  $f$ , which is related to the partition function  $\mathcal{Z}$  as

$$f = -\frac{T}{N_s} \ln \mathcal{Z}, \quad (C1)$$

$$\mathcal{Z} = \text{Tr} e^{-\beta \hat{H}} = \prod_k \text{Tr} e^{-\beta \hat{H}_k} = \prod_k \left( \sum_{j=1}^{16} e^{-\beta E_k(j)} \right).$$

Here, one notes that the partition function is easy to calculate since each  $k$  state contributes independently. Then,

FIG. 17. Spectral function of  $f$  electron  $A_f(k, \omega)$  with  $E_f = -2$  on a square lattice. (a) HI with  $U = 0.5, \mu = -1$  (we choose  $V = 2$  to enhance the visibility of HI). (b) MI with  $U = 12, \mu = 10$ . (c) CM with  $U = 6, \mu = 2$ .



the typical thermodynamic quantity, i.e., the heat capacity, is calculated by the standard thermodynamic relation  $C_V = -T \frac{\partial^2 f}{\partial T^2}$ , which is shown in Fig. 15. In addition to  $C_V$ , one can also calculate spin susceptibility  $\chi_s$  if inserting the Zeeman energy term  $\hat{H}_h = -h\hat{S}_k^z = -\frac{h}{2}(\hat{c}_{k\uparrow}^\dagger \hat{c}_{k\uparrow} - \hat{c}_{k\downarrow}^\dagger \hat{c}_{k\downarrow} + \hat{f}_{k\uparrow}^\dagger \hat{f}_{k\uparrow} - \hat{f}_{k\downarrow}^\dagger \hat{f}_{k\downarrow})$  into Hamiltonian  $\hat{H}_k$ . Then, it follows that the magnetization  $M = -\frac{\partial f}{\partial h}$  and  $\chi_s = \frac{\partial M}{\partial h} = -\frac{\partial^2 f}{\partial h^2}$ .

#### APPENDIX D: SPECTRAL FUNCTION OF 2D SQUARE LATTICE

Here, in Figs. 16 and 17, we show spectral function for the  $c$  and  $f$  electron [ $A_c(k, \omega)$ ,  $A_f(k, \omega)$ ] on a 2D square lattice, and one can see that it is similar to the one on a 1D model. [The momentum  $k$  is chosen from  $(0, 0)$  to  $(\pi, \pi)$ ,  $(\pi, \pi)$  to  $(\pi, 0)$ , and  $(\pi, 0)$  to  $(0, 0)$ .]

- 
- [1] S. Sachdev and J. Ye, *Phys. Rev. Lett.* **70**, 3339 (1993).
- [2] J. Maldacena and D. Stanford, *Phys. Rev. D* **94**, 106002 (2016).
- [3] D. Chowdhury, A. Georges, O. Parcollet, and S. Sachdev, *Rev. Mod. Phys.* **94**, 035004 (2022).
- [4] A. Kitaev, *Ann. Phys. (NY)* **303**, 2 (2003).
- [5] A. Kitaev, *Ann. Phys. (NY)* **321**, 2 (2006).
- [6] Y. Zhou, K. Kanoda, and T.-K. Ng, *Rev. Mod. Phys.* **89**, 025003 (2017).
- [7] C. Prosko, S.-P. Lee, and J. Maciejko, *Phys. Rev. B* **96**, 205104 (2017).
- [8] Y. Zhong, Y.-F. Wang, and H.-G. Luo, *Phys. Rev. B* **88**, 045109 (2013).
- [9] A. Smith, J. Knolle, D. L. Kovrizhin, and R. Moessner, *Phys. Rev. Lett.* **118**, 266601 (2017).
- [10] Z. Chen, X. Li, and T. K. Ng, *Phys. Rev. Lett.* **120**, 046401 (2018).
- [11] Y. Hatsugai and M. Kohmoto, *J. Phys. Soc. Jpn.* **61**, 2056 (1992).
- [12] G. Baskaran, *Mod. Phys. Lett. B* **05**, 643 (1991).
- [13] Y. Hatsugai, M. Kohmoto, T. Koma, and Y.-S. Wu, *Phys. Rev. B* **54**, 5358 (1996).
- [14] P. W. Phillips, C. Setty, and S. Zhang, *Phys. Rev. B* **97**, 195102 (2018).
- [15] L. Yeo and P. W. Phillips, *Phys. Rev. D* **99**, 094030 (2019).
- [16] P. W. Phillips, L. Yeo, and E. W. Huang, *Nat. Phys.* **16**, 1175 (2020).
- [17] K. Yang, *Phys. Rev. B* **103**, 024529 (2021).
- [18] H.-S. Zhu, Z. Li, Q. Han, and Z. D. Wang, *Phys. Rev. B* **103**, 024514 (2021).
- [19] J. Zhao, L. Yeo, E. W. Huang, and P. W. Phillips, *Phys. Rev. B* **105**, 184509 (2022).
- [20] C. Setty, [arXiv:2105.15205](https://arxiv.org/abs/2105.15205).
- [21] P. Mai, B. Feldman, and P. W. Phillips, [arXiv:2207.01638](https://arxiv.org/abs/2207.01638).
- [22] E. W. Huang, G. La Nave and P. W. Phillips, *Nat. Phys.* **18**, 511 (2022).
- [23] Y. Li, V. Mishra, Y. Zhou, and F.-C. Zhang, *New J. Phys.* (2022).
- [24] C. Setty, *Phys. Rev. B* **101**, 184506 (2020).
- [25] C. Setty, *Phys. Rev. B* **103**, 014501 (2021).
- [26] J. Bardeen, L. N. Cooper, and J. R. Schrieffer, *Phys. Rev.* **108**, 1175 (1957).
- [27] H. Tsunetsugu, M. Sigrist, and K. Ueda, *Rev. Mod. Phys.* **69**, 809 (1997).
- [28] M. Dzero, K. Sun, V. Galitski, and P. Coleman, *Phys. Rev. Lett.* **104**, 106408 (2010).
- [29] M. Dzero, K. Sun, P. Coleman, and V. Galitski, *Phys. Rev. B* **85**, 045130 (2012).
- [30] M. A. Griffith, M. A. Continentino, and T. O. Puel, *Phys. Rev. B* **99**, 075109 (2019).
- [31] M. Dzero, J. Xia, V. Galitski, and P. Coleman, *Annu. Rev. Condens. Matter Phys.* **7**, 249 (2016).
- [32] A. Ghazaryan, E. M. Nica, O. Erten, and P. Ghaemi, *New J. Phys.* **23**, 123042 (2021).
- [33] P. Ghaemi and T. Senthil, *Phys. Rev. B* **75**, 144412 (2007).
- [34] P. Ghaemi, T. Senthil, and P. Coleman, *Phys. Rev. B* **77**, 245108 (2008).
- [35] M. Vekić, J. W. Cannon, D. J. Scalapino, R. T. Scalettar, and R. L. Sugar, *Phys. Rev. Lett.* **74**, 2367 (1995).
- [36] K. Masuda and D. Yamamoto, *Phys. Rev. B* **91**, 104508 (2015).
- [37] T. Schäfer, A. A. Katanin, M. Kitatani, A. Toschi, and K. Held, *Phys. Rev. Lett.* **122**, 227201 (2019).
- [38] D. Sherrington and S. Kirkpatrick, *Phys. Rev. Lett.* **35**, 1792 (1975).
- [39] P. Coleman, *Introduction to Many Body Physics* (Cambridge University Press, Cambridge, 2015).
- [40] C. Pépin, *Phys. Rev. Lett.* **98**, 206401 (2007).
- [41] J. M. Luttinger, *Phys. Rev.* **119**, 1153 (1960).
- [42] J. M. Luttinger and J. C. Ward, *Phys. Rev.* **118**, 1417 (1960).
- [43] M. Oshikawa, *Phys. Rev. Lett.* **84**, 3370 (2000).
- [44] D. V. Else, R. Thorngren, and T. Senthil, *Phys. Rev. X* **11**, 021005 (2021).
- [45] I. Dzyaloshinskii, *Phys. Rev. B* **68**, 085113 (2003).
- [46] X. G. Wen and Q. Niu, *Phys. Rev. B* **41**, 9377 (1990).
- [47] T. Senthil and M. P. A. Fisher, *Phys. Rev. B* **63**, 134521 (2001).
- [48] M. Oshikawa and T. Senthil, *Phys. Rev. Lett.* **96**, 060601 (2006).
- [49] J. B. Kogut, *Rev. Mod. Phys.* **51**, 659 (1979).
- [50] M. Continentino, *Quantum Scaling in Many-Body Systems* (Cambridge University Press, Cambridge, 2017).
- [51] C. Vitoriano, L. B. Bejan, A. M. S. Macêdo, and M. D. Coutinho-Filho, *Phys. Rev. B* **61**, 7941 (2000).
- [52] S. C. Zhang, T. H. Hansson, and S. Kivelson, *Phys. Rev. Lett.* **62**, 82 (1989).
- [53] P. A. Lee, N. Nagaosa, and X.-G. Wen, *Rev. Mod. Phys.* **78**, 17 (2006).
- [54] T. Giamarchi, *Quantum Physics in One Dimension* (Oxford University Press, Cambridge, 2003).
- [55] P. Di Francesco, P. Mathieu, and D. Senechal, *Conformal Field Theory* (Springer-Verlag, 1997).
- [56] S. Florens and A. Georges, *Phys. Rev. B* **70**, 035114 (2004).
- [57] A. Rüegg, S. D. Huber, and M. Sigrist, *Phys. Rev. B* **81**, 155118 (2010).
- [58] M. Yamanaka, M. Oshikawa, and I. Affleck, *Phys. Rev. Lett.* **79**, 1110 (1997).
- [59] G. Li *et al.*, *Science* **346**, 1208 (2014).

- [60] B. S. Tan *et al.*, *Science* **349**, 287 (2015).
- [61] Z. Xiang *et al.*, *Science* **362**, 65 (2018).
- [62] J. Knolle and N. R. Cooper, *Phys. Rev. Lett.* **115**, 146401 (2015).
- [63] L. Zhang, X.-Y. Song, and F. Wang, *Phys. Rev. Lett.* **116**, 046404 (2016).
- [64] P. S. Riseborough and Z. Fisk, *Phys. Rev. B* **96**, 195122 (2017).
- [65] G. Baskaran, [arXiv:1507.03477](https://arxiv.org/abs/1507.03477).
- [66] C. M. Varma, *Phys. Rev. B* **102**, 155145 (2020).
- [67] O. Erten, P. Ghaemi, and P. Coleman, *Phys. Rev. Lett.* **116**, 046403 (2016).
- [68] J. Knolle and N. R. Cooper, *Phys. Rev. Lett.* **118**, 096604 (2017).
- [69] P. Rao and I. Sodemann, *Phys. Rev. B* **100**, 155150 (2019).
- [70] Y. Zhong, Y. Liu, and H.-G. Luo, *Eur. Phys. J. B* **90**, 147 (2017).
- [71] F. T. Lisandrini, A. M. Lobos, A. O. Dobry, and C. J. Gazza, *Phys. Rev. B* **96**, 075124 (2017).
- [72] Z. Luo, M. Ferrero, D.-X. Yao, and W. Wu, *Phys. Rev. B* **104**, L161119 (2021).
- [73] P. Zanardi and N. Paunković, *Phys. Rev. E* **74**, 031123 (2006).
- [74] A. F. Albuquerque, F. Alet, C. Sire, and S. Capponi, *Phys. Rev. B* **81**, 064418 (2010).